Inorg. Chem. **2004**, *43*, 4289–4299

Molecular Structure and Vibrational Spectra of Spin-Crossover Complexes in Solution and Colloidal Media: Resonance Raman and Time-Resolved Resonance Raman Studies

Clare Brady,[†] Philip L. Callaghan,[†] Zbigniew Ciunik,[‡] Colin G. Coates,[†] Anders Døssing,[§] Alan Hazell,[||] John J. McGarvey,*[,†] Sabine Schenker,[⊥] Hans Toftlund,[⊥] Alfred X. Trautwein,[#] Heiner Winkler,[#] and Juliusz A. Wolny[‡,#]

School of Chemistry, Queens University Belfast, Stranmillis Road, Belfast BT9 5AG, Northern Ireland, Wydział Chemii, Uniwersytet Wrocławski, ul. F Joliot-Curie 14, 50383 Wrocław, Poland, Institut of Chemistry, University of Copenhagen, Universitetparken 5, DK-2100 Copenhagen Ø, Denmark, Department of Chemistry, Århus University, 8000 Århus C, Denmark, Kemisk Institut, Syddansk Universitet, Campusvej 55, 5230 Odense M, Denmark, and Institut für Physik, Universität zu Lübeck, Ratzeburger Allee 160, D-23538 Lübeck, Germany

Received February 14, 2004

The spin-crossover system $[Fe(btpa)](PF_6)_2$ (btpa = *N*,*N*,*N*′,*N*′-tetrakis(2-pyridylmethyl)-6,6′-bis(aminomethyl)-2,2′-bipyridine) and the predominantly low-spin species $[Fe(b(bdpa))](PF_6)_2$ ((b(bdpa) = *N*,*N*′-bis(benzyl)-*N*,*N*′-bis(2-pyridylmethyl)-6,6′-bis(aminomethyl)-2,2′-bipyridine) have been characterized by means of X-ray diffraction. The unit cell of $[Fe(btpa)](PF_6)_2$ contains two crystallographically independent molecules revealing octahedral low-spin and quasi-seven-coordinated high-spin structures. The unit cell of $[Fe(b(bdpa))](PF_6)_2$ contains two crystallographically independent molecules one of which corresponds to a low-spin structure, while the other reveals a disordering. On the basis of magnetic susceptibility and Mössbauer measurements, it has been proposed that this disorder involves low-spin and high-spin six-coordinated molecules. The structures of $[Zn(btpa)](PF_6)_2$ and $[Ru(btpa)](PF_6)_2$ have been determined also. Pulsed laser photoperturbation, coupled here with time-resolved resonance Raman spectroscopy (TR^3), has been used to investigate, for the first time by this technique, the relaxation dynamics in solution on nanosecond and picosecond time scales of low-spin, LS (^1A) → high-spin, HS (^5T) electronic spin-state crossover in these Fe(II) complexes. For the nanosecond experiments, use of a probe wavelength at 321 nm, falling within the π–π^* transition of the polypyridyl backbone of the ligands, enabled the investigation of vibrational modes of both LS and HS isomers, through coupling to spin-state-dependent angle changes of the backbone. Supplementary investigations of the spin-crossover (SCO) equilibrium in homogeneous solution and in colloidal media assisted the assignment of prominent features in the Raman spectra of the LS and HS isomers. The relaxation data from the nanosecond studies confirm and extend earlier spectrophotometric findings, (Schenker, S.; Stein, P. C.; Wolny, J. A.; Brady, C.; McGarvey, J. J.; Toftlund, H.; Hauser, A. *Inorg. Chem.* **2001**, *40*, 134), pointing to biphasic spin-state relaxation in the case of $[Fe(btpa)](PF_6)_2$ but monophasic in the case of $[Fe(b(bdpa))](PF_6)_2$. The picosecond results suggest an early process complete in 20 ps or less, which is common to both complexes and possibly includes vibrational relaxation in the initially formed $^5T_2$ state.

Introduction

Cambi et al. were the first to report the phenomenon of spin-state crossover in Fe(III) complexes some 70 years ago.[2] It was almost 30 years later that the effect was also demonstrated in Fe(II) systems.[3] While a good deal of attention in the spin-crossover area focuses on Fe(II) complexes in the solid state,[4] studies in dilute solution[1] are also important, not only because they permit study of the intramolecular processes in the absence of intermolecular effects but in addition because investigation of the dynamics

* Author to whom correspondence should be addressed. E-mail: j.mcgarvey@qub.ac.uk.
[†] Queens University Belfast.
[‡] Uniwersytet Wrocławski.
[§] University of Copenhagen.
[||] Århus University.
[⊥] Syddansk Universitet.
[#] Universität zu Lübeck.

(1) Schenker, S.; Stein, P. C.; Wolny, J. A.; Brady, C.; McGarvey, J. J.; Toftlund, H.; Hauser, A. *Inorg. Chem.* **2001**, *40*, 134.

10.1021/ic049809t CCC: $27.50
Published on Web 06/18/2004

of spin equilibria in solution provides a convenient means of probing intersystem crossing (ISC) processes, effectively under ground electronic state conditions.[5]

Time-resolved relaxation studies of spin-crossover systems in solution have been reviewed recently.[6] The work presented here is the first study in which the laser photoperturbation method has been coupled with time-resolved resonance Raman spectroscopy (TR^3) to probe the spin-state relaxation process.

One of the systems under investigation is $[Fe(btpa)](PF_6)_2$. The btpa ligand may be regarded as a dimeric form of tpa (tris(2-pyridylmethyl)amine) ligand. The spin-crossover properties of the iron(II) complex of this ligand have been extensively studied.[7] Btpa is also related to Lehn's cryptate bpy*bpy*bpy[8] (where bpy = 2,2-bipyridine), since it may be envisaged as a bpy cage where two bars have been cut. The resulting ligand is more flexible than the cage and can form complexes with many transition metal ions.[9] The btpa is potentially octadentate, with a bipyridyl backbone and four pendent pyridyl arms, of which only two are coordinated to the central metal ion.

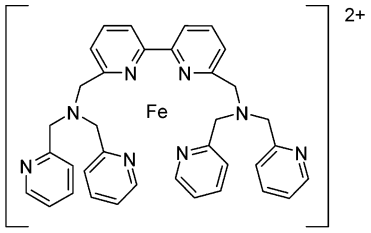

$[Fe(btpa)]^{2+}$

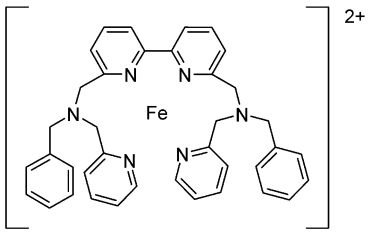

$[Fe(b(bdpa))]^{2+}$

In previous work we reported flash-photolysis studies of $[Fe(btpa)](PF_6)_2$, biphasic relaxation kinetics being observed following the light-induced population of the HS state.[1] The fast process was assigned to direct $^5T_2 \rightarrow {}^1A_1$ relaxation, while the slow process, which is the slowest light-induced relaxation process observed so far for an Fe(II) spin-crossover complex in solution at ambient temperature, was assigned to a coupling of the $^5T_2 \rightarrow {}^1A_1$ relaxation to a rearrangement of the iron pyridyl coordination sphere. In this work, we have used the TR^3 technique over a time range spanning 9 orders of magnitude, from picoseconds to microseconds, to probe changes in the resonance Raman spectra as a function of spin state and thus to monitor the spin-crossover relaxation for $[Fe(btpa)](PF_6)_2$ and the analogous system, $[Fe(b(bdpa))](PF_6)_2$, where the uncoordinated pyridyl groups are replaced by benzyl groups. To underpin the findings from the TR^3 work, variable-temperature resonance Raman (RR) and surface-enhanced resonance Raman spectra (SERRS) were also recorded.

Experimental Section

Preparation of Compounds. HPLC grade solvents were used as obtained without further purification. The synthesis of $[Fe(btpa)](PF_6)_2$ and $[Fe(b(bdpa))](PF_6)_2$ has been described previously.[1]

$[Ru(btpa)](PF_6)_2 \cdot H_2O$. A 100 mg amount of $Ru(dmso)_4Cl_2$ and 121 mg of btpa (0.00021 mol) were boiled in 400 mL of ethanol overnight. The solvent was removed, and the resulting oil was dissolved in ca. 15 mL of water. Addition of an aqueous solution of ammonium hexafluorophosphate resulted in precipitation of brown powder, which was filtered off and dried in air. The product was purified by thick-layer chromatography following the procedure previously described.[10] Recrystallization from CH_2Cl_2/ligroine yielded 91 mg of brown crystals (44%).

Anal. Calcd for $C_{36}H_{36}N_8OF_{12}P_2Ru$: H, 3.67; C, 43.72; N, 11.34. Found: H, 3.74; C, 43.64; N, 11.25. UV spectrum: $\lambda_{max} = 485$ nm, sh 455 nm. Mass spectrum (FAB) (*m*/*z*): 825, $[Ru(btpa)](PF_6)^+$ (100%); 679, $[Ru(btpa)]^+$ (55%).

$[Zn(btpa)](PF_6)_2 \cdot 1/2(H_2O)$. A 72 mg amount of $ZnSO_4 \cdot 7H_2O$ (0.00025 mol) in a minimal amount of water was mixed with 145 mg of btpa (0.00025 mol) in 3 mL of methanol and stirred for 10 min. Addition of a saturated solution of ammonium hexafluorophosphate yielded a white precipitate, which was filtered off, washed with water, and dried in air. Yield: 200 mg (85%). Anal. Calcd for $C_{36}H_{35}F_{12}N_8P_2ZnO_{0.5}$: H, 3.75; C, 45.90; N, 11.90. Found: H, 3.69; C, 45.77; N, 11.88.

(2) (a) Cambi, L.; Cagnasso, A. *Atti. Accad. Naz. Lincei* **1931**, *13*, 809. (b) Cambi, L.; Szego, L.; Cagnasso, A. *Atti. Accad. Naz. Lincei* **1932b**, *15*, 329.

(3) Baker, W. A.; Bobonich, H. M. *Inorg. Chem.* **1964**, *3*, 1184.

(4) (a) König, E. *Coord. Chem. Rev.* **1968**, *3*, 471. (b) Goodwin, H. A. *Coord. Chem. Rev.* **1976**, *18*, 293. (c) Gütlich, P. *Struct. Bonding (Berlin)* **1981**, *44*, 83. (d) Toftlund, H. *Coord. Chem. Rev.* **1989**, *94*, 67. (e) Gütlich, P.; Hauser, A.; Spiering, H. *Angew. Chem., Int. Ed. Engl.* **1994**, *33*, 20. (f) Gütlich, P.; Garcia, Y.; Goodwin, H. A. *Chem. Soc. Rev.* **2000**, *29*, 419.

(5) Beattie, J. K. *Adv. Inorg. Chem.* **1988**, *32*, 1.

(6) Brady, C.; McGarvey, J. J.; McCusker, J. K.; Toftlund, H.; Hendrickson, D. N. *Spin Crossover in Transition Metal Complexes. Topics in Current Chemistry*; Gütlich, P., Goodwin, H., Eds.; Springer-Verlag: New York, in press.

(7) (a) Hazell, A.; Jensen, K. B.; McKenzie, C. J.; Toftlund, H. *Inorg. Chem.* **1994**, *33*, 3127. (b) Toftlund. H.; Ishiguro, S. *Inorg. Chem.* **1989**, *28*, 2236. (c) Hojland, F.; Toftlund, H.; Yde-Andersen, S. *Acta Chem. Scand.* **1983**, *A37*, 251. (d) Grünsteudel, H.; Paulsen, H.; Meyer-Klaucke, W.; Winkler, H.; Trautwein, A. X.; Grünsteudel, H. F.; Baron, A. Q. R.; Chumakov, A. I.; Ruffer, R.; Toftlund, H. *Hyperfine Interact.* **1998**, *113*, 311. (e) Grünsteudel, H.; Paulsen, H.; Winkler, H.; Trautwein, A. X.; Toftlund, H. *Hyperfine Interact.* **1999**, *123*, 841. (f) Paulsen, H.; Winkler, H.; Trautwein, A. X.; Grünsteudel, H.; Rusanov, V.; Toftlund, H. *Phys. Rev. B* **1999**, *59*, 975. (g) Paulsen, H.; Grünsteudel H.; Meyer-Klaucke, W.; Gerdan, M.; Grünsteudel, H. F.; Chumakov, A. I.; Ruffer, R.; Winkler, H.; Toftlund, H.; Trautwein, A. X. *Eur. Phys. J. B* **2001**, *23*, 463. (h) Winkler, H.; Trautwein, A. X. *Spin Crossover in Transition Metal Complexes. Topics in Current Chemistry*; Gütlich, P., Goodwin, H., Eds.; Springer-Verlag: New York, in press.

(8) Caron, A.; Giulhelm, J.; Riche, C.; Pascard, C.; Alpha, B.; Lehn, J.-M.; Rodriguez-Ubis, J.-C. *Helv. Chim. Acta* **1985**, *68*, 1577.

(9) (a) Døssing, A.; Hazell, A.; Toftlund, H. *Acta Chem. Scand.* **1996**, *50*, 95. (b) Døssing, A.; Toftlund, H.; Hazell, A.; Bourassa, J.; Ford, P. C. *J. Chem. Soc., Dalton Trans.* **1997**, 335. (c) Døssing, A.; Engberg, P.; Hazell, R. *Inorg. Chim. Acta* **1998**, *268*, 159. (d) Døssing, A.; Kristensen, S. M.; Toftlund, H.; Wolny, J. A. *Acta Chem. Scand.* **1999**, *53*, 575. (e) Døssing, A.; Sokolnicki, J.; Riehl, J. P.; Legendziewicz, J. *J. Alloys Compd.* **2002**, 341.

(10) Bjernemose, J.; Hazell, A.; McKenzie, C. J.; McMahon, M. F.; Nielsen, L. P.; Raithby, P. R.; Simonsen, O.; Toftlund, H.; Wolny, J. A. *Polyhedron* **2003**, *22*, 875.

Table 1. Bond Distances and Angles for [Ru(btpa)]$(PF_6)_2$ (**1**), [Fe(btpa)]$(PF_6)_2$ (**2**), and [Zn(btpa)]$(PF_6)_2$ (**3**)

atoms			X for **1**·H_2O		X for **2**						
X	N		Ru	RuA	Fe295	Fe200	Fe120	FeA295	FeA200	FeA120	X for **3**·0.5C_3H_6O: Zn
M	N10		2.173(3)	2.178(3)	2.112(7)	2.102(7)	2.117(9)	2.355(8)	2.342(8)	2.344(7)	2.424(3)
M	N20		2.182(3)	2.186(3)	2.116(7)	2.113(7)	2.121(9)	2.339(8)	2.325(9)	2.365(12)	2.374(3)
M	N17		2.062(3)	2.067(3)	1.957(8)	1.970(8)	1.958(9)	2.139(8)	2.124(9)	2.127(12)	2.086(3)
M	N27							3.109(10)	3.081(10)	3.102(15)	
M	N37		1.965(3)	1.959(3)	1.892(7)	1.888(7)	1.896(9)	2.206(10)	2.175(10)	2.237(15)	2.114(3)
M	N47		1.952(3)	1.955(3)	1.870(8)	1.868(7)	1.882(9)	2.190(9)	2.205(9)	2.202(13)	2.090(3)
M	N67		2.081(3)	2.059(3)	1.981(8)	1.984(7)	1.975(9)	2.126(8)	2.113(8)	2.112(11)	2.083(3)
N	X	N									
N10	M	N20	115.2(1)	115.7(1)	112.0(3)	112.0(3)	111.4(3)	140.5(3)	140.7(3)	140.8(4)	131.5(1)
N10	M	N17	79.6(1)	80.9(1)	83.5(3)	82.7(3)	82.9(4)	77.1(3)	77.0(3)	76.8(4)	76.8(1)
N10	M	N27						60.2(3)	60.5(3)	61.1(4)	
N10	M	N37	81.8(1)	81.7(1)	83.2(3)	82.8(3)	83.3(4)	74.0(4)	73.5(4)	73.7(5)	75.0(1)
N10	M	N47	163.0(1)	162.5(1)	164.3(3)	165.2(3)	164.8(4)	145.7(4)	145.6(4)	145.5(5)	151.0(1)
N10	M	N67	100.0(1)	96.2(1)	96.0(3)	96.1(3)	96.4(3)	95.2(3)	94.9(4)	95.1(4)	90.3(1)
N17	M	N20	96.3(1)	101.0(1)	95.3(3)	94.9(3)	95.1(4)	104.7(3)	105.2(3)	106.3(5)	94.9(1)
N17	M	N27						87.7(3)	87.2(3)	87.9(5)	
N17	M	N37	89.6(1)	84.7(1)	88.4(3)	88.2(3)	88.0(4)	83.5(4)	83.4(4)	82.4(6)	95.2(1)
N17	M	N47	99.1(1)	95.8(1)	96.0(3)	95.8(3)	95.6(4)	97.5(3)	97.6(4)	97.4(5)	109.9(1)
N17	M	N67	175.3(1)	177.1(1)	176.3(3)	175.7(3)	177.0(4)	170.0(4)	169.3(4)	170.1(5)	153.6(1)
N20	M	N27						80.3(3)	80.3(3)	79.9(4)	
N20	M	N37	162.7(1)	162.3(1)	164.7(3)	165.1(3)	165.2(4)	145.3(3)	145.6(3)	145.1(4)	153.4(1)
N20	M	N47	81.8(1)	81.9(1)	83.7(3)	82.8(3)	83.8(4)	73.8(3)	73.7(3)	73.6(5)	77.1(1)
N20	M	N67	79.6(1)	80.4(1)	82.1(3)	81.7(3)	82.4(4)	77.1(3)	76.5(3)	76.3(4)	76.4(1)
N27	M	N37						134.2(3)	133.9(3)	134.8(4)	
N27	M	N47						154.1(3)	153.8(3)	153.4(5)	
N27	M	N67						82.9(3)	82.6(3)	83.2(4)	
N37	M	N47	81.2(1)	80.8(1)	81.1(3)	82.4(3)	81.5(4)	71.7(4)	72.2(4)	71.8(5)	76.3(1)
N37	M	N67	94.9(1)	94.7(1)	94.8(3)	95.7(3)	94.8(4)	100.6(4)	101.2(4)	100.9(5)	103.6(1)
N47	M	N67	82.7(1)	86.9(1)	86.3(3)	86.4(3)	85.9(4)	92.5(3)	93.1(3)	92.5(5)	92.7(1)

The samples for SERRS studies were prepared by adding ~1 mg of solid complex to 500 μL of aqueous silver colloid, prepared according to a literature procedure.[11]

Crystal Structure Analyses. Crystals of [Fe(btpa)]$(PF_6)_2$ were grown with considerable difficulties by slow diffusion from a CH_2Cl_2 solution covered with a layer of hexane; for [Fe(b(bdpa))]$(PF_6)_2$, crystals were grown from acetone/water while in the case of [Zn(btpa)]$(PF_6)_2$·0.5(C_3H_6O) crystals were grown from CH_2Cl_2/acetone/diethyl ether mixtures. Crystals of [Ru(btpa)]$(PF_6)_2$·H_2O were obtained directly from synthesis.

Crystals of [Fe(btpa)]$(PF_6)_2$, [Ru(btpa)]$(PF_6)_2$·H_2O, and [Zn(btpa)]$(PF_6)_2$·0.5C_3H_6O were mounted on a Bruker-Smart CCD diffractometer, and data were collected at 120 K for all three samples. Additional data sets were collected at 200 and 295 K for [Fe(b(bdpa))]$(PF_6)_2$. Crystal data and details of refinement are listed in Table S1, Supporting Information. Data were collected with ω-scans and corrected for Lorentz and polarization effects[12] and for absorption. The structures were solved by direct methods using SIR97[13] and refined by the method of least-squares on *F*. Hydrogen atoms of the ligands and of the acetone solvate were kept fixed at calculated positions while those of the water molecule were kept fixed at the positions determined from a difference synthesis. The [Fe(b(bdpa))]$(PF_6)_2$ complex gave very few reflections at room temperature; anisotropic displacement factors for the cations and the PF_6^- anions were modeled by **T**, **L**, and **S** tensors[14] with an extra libration about the C−C bonds of the dangling methyl pyridine groups to reduce the number of parameters. Cooling the crystal to 120 K gave only a few more reflections, and whereas the displacement ellipsoids for the low-spin complex and for the anions become smaller, those for the high-spin complex became more elongated, suggesting disorder. Consequently, for the 120 K structure the high-spin cation was modeled as two identical groups related by a translation and rotation. (The splitting of the Fe atom was 0.58(1) Å.) A third data set at 200 K from a new crystal showed intermediate behavior. Programs, other than those referenced, were from KRYSTAL.[15] Selected bond distances and angles are listed in Table 1.

X-ray data for [Fe(b(bdpa))]$(PF_6)_2$ were collected at low temperature using an Oxford Cryosystem device on a Kuma KM4CCD κ-axis diffractometer with graphite-monochromated Mo Kα radiation (λ = 0.710 73 Å). Crystal data are given in Table S1, together with refinement details. The crystal was positioned at 65 mm from the CCD camera. A total of 612 frames were measured at 0.75° intervals with a counting time of 20 s. Accurate cell parameters were determined and refined by least-squares fit of 2900 of the strongest reflections. The data were corrected for Lorentz and polarization effects. No absorption correction was applied. Data reduction and analysis were carried out with the Oxford Diffraction (Wrocław, Poland) Sp. z o.o (formerly Kuma Diffraction, Wrocław, Poland) programs. The structure was solved by direct methods (program SHELXS97[16]) and refined by the full-matrix least-squares method on all F^2 data using the SHELXL97 programs.[17] The low quality of the measured crystal meant that only part of the non-hydrogen atoms (Fe, P, and F) were refined with anisotropic displacement parameters; hydrogen atoms were included from geometry of molecules and $\Delta\rho$ maps. They were treated as riding atoms.

Crystallographic data (excluding structure factors) for the structures in this paper have been deposited with the Cambridge Crystallographic Data Centre as supplementary publications nos.

(11) Lee, P. C.; Meisel, D. J. *J. Phys. Chem.* **1982**, *86*, 3391.
(12) *SMART, SAINT, and XPREP*; Siemens Analytical X-ray Instruments Inc.: Madison, WI, 1995.
(13) Altomare, A.; Cascarano, G.; Giacovazzo, C.; Guagliardi, A.; Moliterni, A. G. G.; Polidori, M. C. G.; Camalli, M.; Spagna, R. *DIR 97*; University of Bari: Bari, Italy, 1997.
(14) Pawley, G. S. *Adv. Struct. Res. Diffr. Methods* **1971**, *4*, 1.
(15) Hazell, A. *KRYSTAL*; Aarhus University: Aarhus, Denmark, 1995.
(16) Sheldrick, G. M. *Acta Crystallogr*. **1990**, *A46*, 467−473.
(17) Sheldrick, G. M. *SHELXL97, program for crystal structure refinement*; University of Göttingen: Göttingen, Germany, 1997.

CCDC 230614−230619. Copies of the data can be obtained, free of charge, on application to CCDC, 12 Union Road, Cambridge CB2 1EZ, U.K. (fax +44 1223 336033 or e-mail deposit@ccdc.cam.ac.uk).

Physical Measurements. UV−vis absorption measurements were made using a HP8453 diode array spectrophotometer. ^{57}Fe Mössbauer spectra were recorded with a conventional spectrometer with a ^{57}Co[Rh] source. The velocity calibration was performed with an "α-Fe" foil at room temperature, for which the hyperfine splitting is known with high accuracy. The measured isomer shifts are referred to this α-Fe standard. The experimental spectra were fitted by a sum of Lorentzian lines using a least-squares procedure.

Time-resolved resonance Raman spectra on the nanosecond time scale were recorded using the two-color pump and probe method with Q-switched Nd:YAG lasers (Spectra Physics models DCR2 and GCR3) as the pump and probe sources. A pump wavelength of 355 nm was employed. For the probe, the laser was coupled to a stimulated Raman wavelength-shifting cell filled with D_2 to provide anti-Stokes output at 321 nm.

The pump/probe time delays were controlled using a digital pulse generator (Stanford Research Instruments SDG535) and monitored on an oscilloscope (Tektronix TDS 350) triggered optically from a fast response photodiode. Pump energy was typically ca. 6 mJ, and probe energy, ca. 0.65 mJ. The pump and probe beams were incident on the sample at 45° to the Raman scattering collection optics. Burn marks taken close to the sample were used to check the relative sizes of the pump and (smaller diameter) probe beams.[18]

Time-resolved spectra were recorded with a gated ICCD (Andor Technology model DH501) coupled to a triple spectrometer of in-house design described previously.[19]

Samples were contained in spinning quartz NMR tubes to minimize the possibility of thermal degradation and/or photodegradation. Sample integrity was confirmed by recording UV−visible absorption spectra before and after Raman measurements. In addition, probe only Raman spectra were recorded at regular intervals.

The picosecond TR^3 studies were carried out at the Central Laser Facility, Rutherford Appleton Laboratory (RAL). The experimental setup in this laboratory has been described previously.[20] It did not prove technically possible to employ a probe wavelength as short as 321 nm, and for the series of spectra reported below, pump and probe wavelengths of 390 nm were selected, with pulse energies of 10 μJ in each case. The Kerr cell gating technique[21] was employed, partly to reduce fluorescence but primarily to eliminate Raman scattering due to the pump beam, operating at the same wavelength as the probe.[20]

The variable-temperature resonance Raman and surface-enhanced resonance Raman spectra were recorded with a CCD detector (Princeton Instruments model LN/UV 1152) coupled to a Jobin-Yvon HR640 spectrometer. The excitation source was an Ar^+ laser (Spectra Physics model 2060/65) with outputs in the visible range 450−528 nm.

Results

Molecular Structure of the Complexes. The molecular representations of both isomers of $[Fe(btpa)](PF_6)_2$ together with the representations of $[Ru(btpa)](PF_6)_2$, $[Zn(btpa)](PF_6)_2$, and $[Fe(b(bdpa))](PF_6)_2$ are shown in Figures 1−3, respectively.

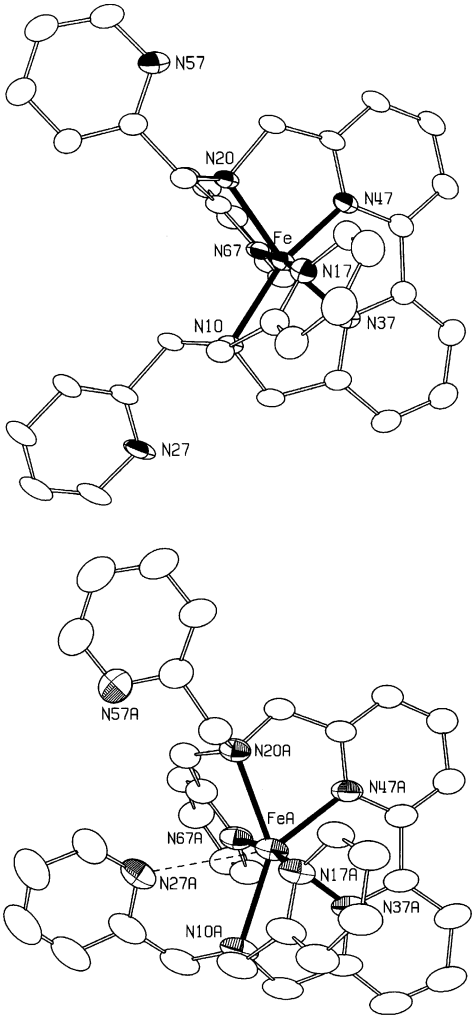

Figure 1. Molecular representations of high-spin (bottom) and low-spin (top) $[Fe(btpa)]^{2+}$ cations.

[Fe(btpa)](PF$_6$)$_2$. The structures determined at temperatures of 295, 200, and 120 K are essentially the same. There are two crystallographically independent molecules of dramatically different structures shown in Figure 1. The upper structure reveals six coordination with bipyridine and sp^3-nitrogens defining the equatorial plane, while two pyridines, each from half of the btpa ligand, coordinate axially. There are two pyridines that remain uncoordinated. The molecule exhibits approximately C_2 symmetry. The lower structure in Figure 1, denoted FeA, displays a much more distorted geometry. The conjugated equatorial angle N10−Fe−N20 of 111.4(3)° for the C_2 molecule (120 K) changes to 140.8(4)° for FeA, while one of the pyridines which was not coordinated in the C_2 molecule moves into the gap thus created and, at a distance of ca. 3.1 Å, is almost within bonding range. Similar distances have been observed in the Fe(II) complex of the potentially octadentate polypicolylamine ligand where two semicoordinated bonds were found.[22]

(18) Brady, C. Ph.D. Thesis, Queens University of Belfast, Belfast, U.K., 2002.
(19) Gordon, K. C.; McGarvey, J. J. *Inorg. Chem.* **1991**, *30*, 2986.
(20) (a) Towrie, M.; Parker, A. W.; Shaikh, W.; Matousek, P. *Meas. Sci. Technol.* **1998**, *9*, 816. (b) Coates, C. G.; Olofsson, J.; Coletti, M.; McGarvey, J. J.; Onfelt, B.; Lincoln, P.; Norden, B.; Tuite, E.; Matousek, P.; Parker, A. W. *J. Phys. Chem. B* **2001**, *105*, 12653.
(21) Matousek, P.; Towrie, M.; Stanley, A.; Parker, A. W. *Appl. Spectrosc.* **1999**, *53*, 1485.
(22) Bu, X.-H.; Lu, S. L.; Zhang, R.-H.; Liu, H.-P.; Liu, Q.-T. *Polyhedron* **2000**, *19*, 431.

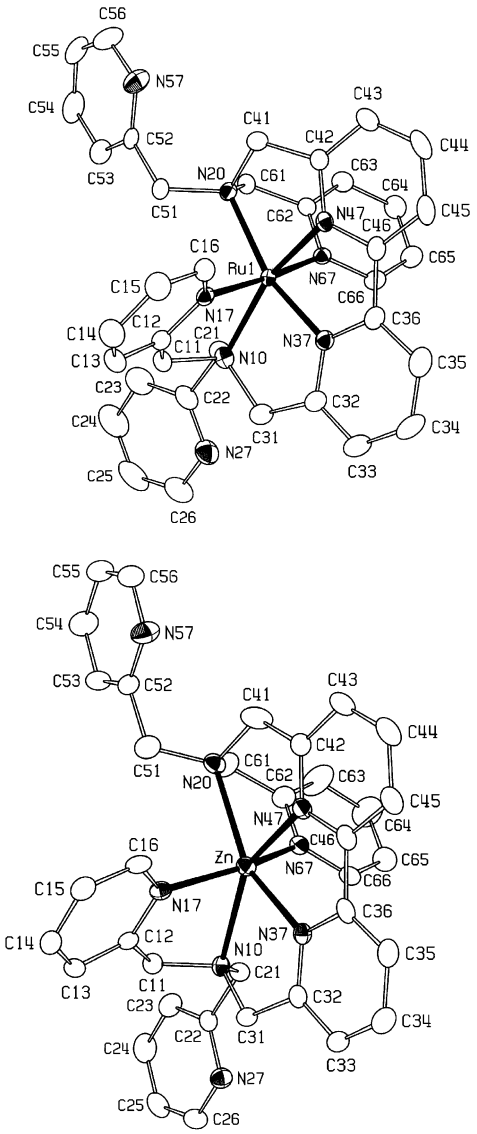

Figure 2. Molecular representation of $[Ru(btpa)]^{2+}$ (top) and $[Zn(btpa)]^{2+}$ (botttom) cations.

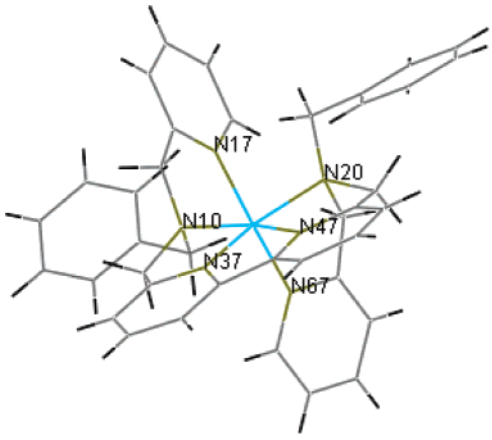

Figure 3. Molecular representation of the $[Fe(b(bdpa))]^{2+}$ cation.

The actual coordination polyhedron of FeA is close to a pentagonal bipyramid.

$[Ru(btpa)](PF_6)_2 \cdot H_2O$. There are two crystallographically independent molecules in the unit cell, yet the differences between them are only minor. The complex is octahedral and displays approximately C_2 symmetry; two pyridines are uncoordinated (Figure 2, top structure). The overall structure and metal−ligand bond lengths are practically identical with those of the low-spin $[Fe(btpa)](PF_6)_2$, the main difference observed being in the value of the conjugated equatorial angle N10−M−N20 which is ca. 3° higher (115.2(1) and 115.7(1)° for two independent molecules) for the ruthenium complex. The NMR spectrum in acetone-d_6 reveals that the observed structure is retained in solution.

$[Zn(btpa)](PF_6)_2 \cdot 0.5C_3H_6O$. The structure of the zinc complex may be regarded as intermediate between those of low-spin $[Fe(btpa)](PF_6)_2$ (and $[Ru(btpa)](PF_6)_2$) and high-spin $[Fe(btpa)](PF_6)_2$. The ligand acts as hexadentate with two pyridines remaining uncoordinated and reveals an approximate C_2 symmetry (Figure 2, bottom structure). However, the overall structure is much more distorted from octahedral geometry, with the angle N10−M−N20 of 131.5(1)° being closer to that of high-spin $[Fe(btpa)](PF_6)_2$. Apart from that, the angle defined by the axial pyridines, N17−Zn−N67, is only 153.6(1)°, compared to the values of 170.1(5) and 177.0(4)° for high-spin and low-spin $[Fe(btpa)](PF_6)_2$, respectively (at 120 K). All metal−ligand bond distances are in the range observed for high-spin $[Fe(btpa)](PF_6)_2$. Thus, the structure is similar to that of high-spin $[Fe(btpa)](PF_6)_2$ with the latter involving a closer approach of one of the two uncoordinated pyridines.

It is noteworthy that for low-spin $[Fe(btpa)](PF_6)_2$ and $[Ru(btpa)](PF_6)_2$ the structures reveal a degree of strain due to distortion from octahedral geometry. This is reflected mainly in the unusually large values of the N10−Me−N20 angle (111−115°). Moreover, significant distortions from regular geometry are seen in the bipyridine moiety.[23] It appears that it is the distorted geometry associated with the closer approach of one of the two uncoordinated pyridines that triggers the high-spin state. Both the flash photolysis[1] and NMR results[24] reveal that the spin equilibrium is much more shifted toward the high-spin state for $[Fe(btpa)](PF_6)_2$ than for its benzyl analogue $[Fe(b(bdpa))](PF_6)_2$.

$[Fe(b(bdpa))](PF_6)_2$. The molecule (Figure 3) reveals a geometry practically identical with that of the low-spin $[Fe(btpa)](PF_6)_2$.[25] In the case of the second compound we obtained a reasonable model of the low-spin molecule, but the refinement process unexpectedly revealed a disorder phenomenon. The difference Fourier map displayed a large

(23) Although in the btpa complexes studied here there is no systematic variation in bow and twist deformations of bipyridine, there is a systematic variation of an in-plane deformation.[38] The α angle reflecting the latter depends on M−N(bipy) distance, changing from 19.6° for low-spin $[Fe(btpa)](PF_6)_2$ and 18.4 and 18.7° for $[Ru(btpa)]^{2+}$ to 12.2 and 10.2° for $[Zn(btpa)]^{2+}$ and high-spin $[Fe(b(bdpa))](PF_6)_2$, respectively. The in-plane distortion relieves the strain at the M−N−C angles.

(24) Susceptibility measurements made by the Evans method show that the magnetic moment of $[Fe(btpa)](PF_6)_2$ varies from 4.0 μ_B at 296 to 4.59 μ_B at 343 K while for $[Fe(b(bdpa)](PF_6)_2$ it changes from 1.52 μ_B at 296 K to 2.146 μ_B at 343 K (CD_3CN).

(25) Bond lengths (Å): Fe−N(bipy), 1.818(6), 1.856(7); Fe−N(sp^3), 2.085(14), 2.128(12); Fe−N(py), 2.003(7), 1.956(7). Bond angle (deg): N(sp^3)−Fe−N′(sp^3), 111.3(4).

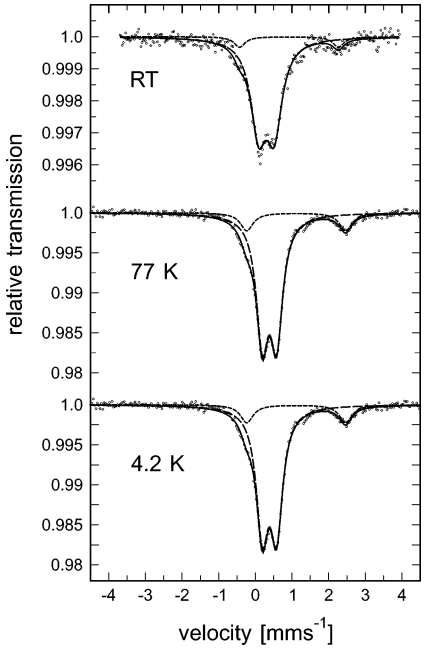

Figure 4. Temperature-dependent Mössbauer spectra of [Fe(b(bdpa))]-$(PF_6)_2$.

number of low maxima in the region of the ligand, making impossible a further refinement with anisotropic displacement parameters.

The magnetic susceptibility data show a weakly temperature-dependent magnetic moment ($\mu = 2.11\ \mu_B$ at 77 K and 2.52 at 293 K) suggesting an approximate 20−25% fraction of the high-spin state over this temperature range. (Magnetic susceptibility data for both [Fe(btpa)]$(PF_6)_2$ and [Fe(b(bdpa))]-$(PF_6)_2$ are given in the Supporting Information, Table S2.) The Mössbauer spectra show a dominant doublet due to a low-spin form with parameters similar to that of low-spin [Fe(btpa)]$(PF_6)_2$ (IS = 0.30, QS = 0.43 mm/s, RT (room temperature), vs Fe). Apart from that, a doublet due to a high-spin form (IS = 1.11, QS = 2.70 mm/s, RT, Fe) is observed across the whole temperature range 4.2−293 K, the relative area of which was found to vary from ca. 16% at 4.2 K, ca. 14% at 77 K, to ca. 8% at 293 K. (Although this appears to be in some disagreement with the above data, it should be remembered that the peak area is not necessarily equal to the mole fraction of the species.) It is noteworthy that (a) the quadrupole splitting of the low-spin doublet increases with increasing temperature and the doublet displays asymmetry at RT, (b) its line width increases with increasing temperature, and (c) the area of the high-spin doublet decreases with increasing temperature. The relevant Mössbauer spectra are shown in Figure 4.

Nanosecond TR^3 Studies. [Fe(btpa)]$(PF_6)_2$ (1). The electronic absorption spectrum of [Fe(btpa)]$(PF_6)_2$ in acetonitrile is dominated in the visible region by the MLCT transition of the low-spin species while the ultraviolet region is dominated by the intraligand bands. For the TR^3 studies a pump wavelength of 355 nm was used to populate the HS state and consequently perturb the LS ↔ HS equilibrium. Since the HS state exhibits weak absorbance throughout the visible region, this makes the choice of probe wavelength more difficult for these spin crossover systems. In the present instance, however, a probe wavelength of 321 nm, within the $\pi-\pi^*$ absorption of the bipyridyl moiety of the btpa ligand, was found to be suitable since it enabled investigation of vibrational modes of both the LS and the HS isomers, as discussed more fully below.

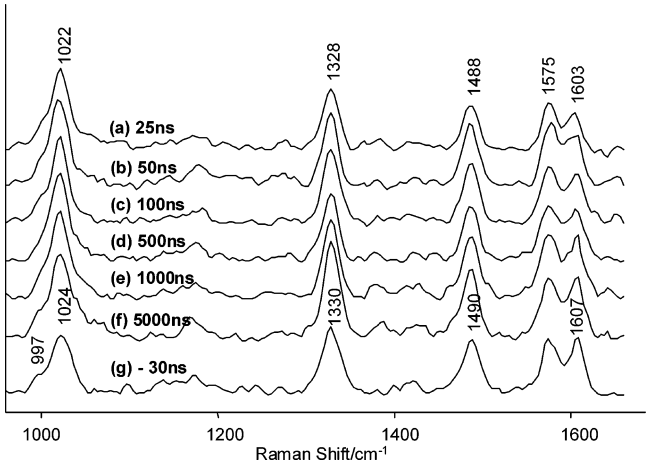

Figure 5. Nanosecond-TR^3 study of [Fe(btpa)]$(PF_6)_2$ in acetonitrile (concentration ca. 5×10^{-4} mol dm^3; pump = 355 nm, 6 mJ; probe = 321 nm, 0.65 mJ).

Results from the nanosecond TR^3 study are illustrated in Figure 5, which displays spectra from which solvent bands have been subtracted. The TR^3 spectra were recorded at a series of pump−probe delay times, with long signal accumulation times and using the maximum achievable probe energies to optimize signal:noise on the recorded traces. A more extended series of measurements covering intermediate as well as the shorter and longer time delays were also recorded (Supporting Information, Figure S3). For the traces shown in Figure 5, the −30 ns spectrum at room temperature (trace g, in effect a "probe-only" experiment since the probe pulse reaches the sample in advance of the pump pulse) contains vibrational features (largely associated with neutral bpy modes[26] of the bipyridyl moiety of the btpa ligand) attributable to both the HS and the LS states. The initial effect of the pump pulse is to deplete the ground state. The actual changes are quite subtle (see kinetic analysis below and ref 27), but the most noticeable effect in the spectra recorded at short time delays (trace a) is the decrease in intensity of the band at 1607 cm^{-1} in the probe-only spectrum. This band grows back in with time, and the system returns to equilibrium on a time scale of a few microseconds. The spectrum recorded at the shortest pump−probe time delay contains predominantly HS features. The subtraction of the spectrum in trace a from that in trace g produces a spectrum, which,

(26) Strommen, D. P.; Mallick, P. K.; Danzer, G. D.; Lumpkin, R. S.; Kincaid, J. R. *J. Phys. Chem.* **1990**, *94*, 1357.

(27) A subroutine within a multivariate analysis program, "The Unscrambler", selected the most correlated spectral peaks from the entire series of spectra (Figure S3) as input. The optimum correlation emerged when the spectra were input in two time segments, 15−100 and 150−5000 ns. Although the procedure here involves a partial least-squares linear regression and is not therefore a kinetic analysis, the appearance of the optimum correlation by taking the data in two time segments is qualitatively consistent with the biphasic decay which emerges from the kinetic analysis.

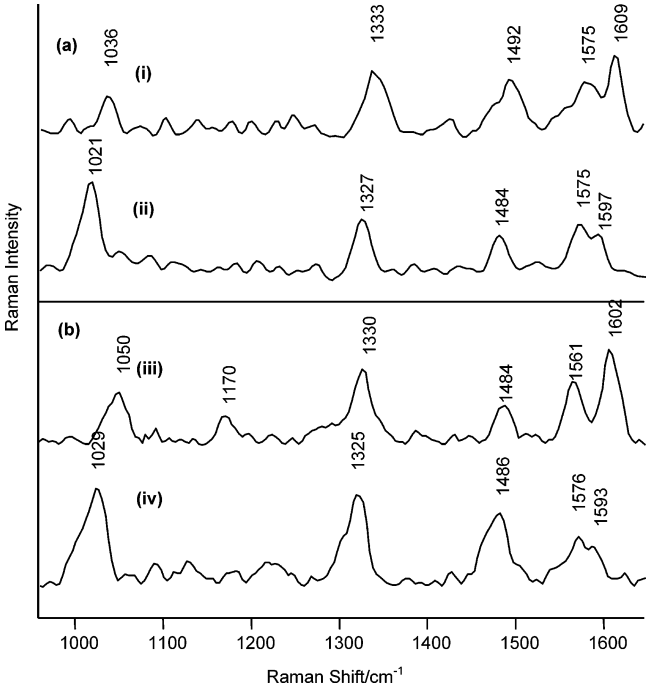

Figure 6. Comparison of (a) representative (i) low-spin (LS) and (ii) high-spin (HS) spectra of $[Fe(btpa)](PF_6)_2$ obtained from subtractions of TR^3 spectra (see text) with (b) Raman spectra of "model" complexes, (iii) $[Ru(btpa)](PF_6)_2$ and (iv) $[Zn(btpa)](PF_6)_2$ obtained at 321 nm.

although noisy, is characteristic of the LS state (Figure 6 a, trace i) while the reverse subtraction yields a spectrum of the HS state (Figure 6a, trace ii). The character of the subtracted spectra is confirmed by the comparison shown in Figure 6b with the spectra (also recorded at a probe wavelength of 321 nm) of the "model" LS and HS complexes referred to above, $[Ru(btpa)](PF_6)_2$ (LS) and $[Zn(btpa)](PF_6)_2$ (HS). The correspondence between the positions of several bands in the spectra of the LS and HS species and those of the respective "model" complexes suggest that the changes observed in the TR^3 spectra of $[Fe(btpa)](PF_6)_2$ reflect subtle changes in the geometry of the bipyridyl unit as the system undergoes spin conversion. The subtractions in the 1330 cm^{-1} region in Figure 6a are compromised somewhat by the proximity in the original spectra of a strong solvent feature near 1300 cm^{-1}, with the result that the subtracted spectra are noisiest at this point. The subtractions do suggest that the shift in the 1330 cm^{-1} band between the HS and LS isomers must be small (<5 cm^{-1}), as indeed is the case for the spectra of the model complexes (Figure 6b).

$[Fe(b(bdpa))](PF_6)_2$. The probe-only spectrum for this complex is virtually identical with that for $[Fe(btpa)](PF_6)_2$, and the spectra recorded at short pump−probe time delays also show changes analogous to those observed for $[Fe(btpa)](PF_6)_2$. Again, as above, scaled subtractions can be used to generate the individual spectra of the LS and HS isomers (spectra not shown). In the case of the $[Fe(b(bdpa))](PF_6)_2$ complex there are no additional pyridyl arms to potentially influence the spectra by their positioning relative to the metal center.

Construction of Kinetic Traces. For the $[Fe(btpa)](PF_6)_2$ complex the relaxation kinetics were investigated by sub-

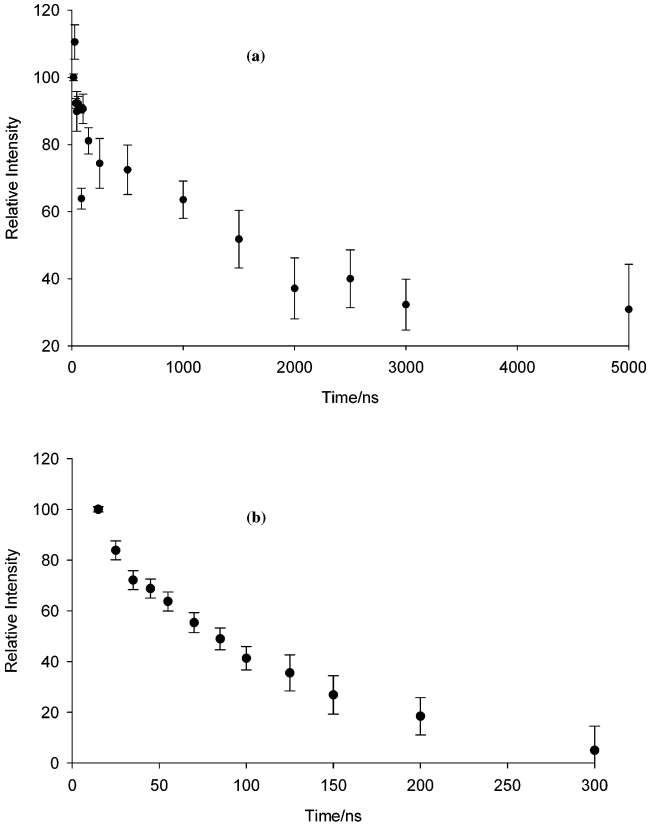

Figure 7. Kinetics traces derived from subtractions of TR^3 data (see text for details): (a) $[Fe(btpa)](PF_6)_2$; (b) $[Fe(b(bdpa))](PF_6)_2$.

tracting spectra recorded at various time delays from that at negative time delay (i.e. probe only) and plotting the intensity of the 1607 cm^{-1} LS feature against time. The more extended series of TR^3 measurements (Figure S3, Supporting Information) were used for this analysis. The resulting kinetic trace (Figure 7a) displays considerable scatter in the individual points (error bars indicate the spectral subtraction errors), reflecting the noise generated in the subtractions (vide supra). An alternative treatment of the data, plotting the 1607/1575 band ratio, gave a qualitative verification of the decay shown in Figure 7a. While TR^3 is not a primary method of choice for investigation of kinetics per se (its use here being to enhance the degree of structural information available through a vibrational probe), the plotted points clearly suggest that the decay is nonexponential.[27] It can be resolved into two processes, the faster characterized by a lifetime of ∼70 ns and the slower having a lifetime of ∼1750 ns. The errors on these numbers are considerable, but the values correlate qualitatively with the lifetimes obtained in the previous flash photolysis study using conventional spectrophotometric detection.[1] A corresponding plot in Figure 7b for the benzyl complex, $[Fe(b(bdpa))](PF_6)_2$, points to a single-exponential process and a relaxation time of 75 ns.

Picosecond Studies on $[Fe(btpa)](PF_6)_2$ and $[Fe(b(bdpa))](PF_6)_2$. Picosecond TR^3 Studies. In the spectra recorded for $[Fe(btpa)](PF_6)_2$, with both pump and probe wavelengths set at 390 nm and an excitation pulse duration of 1 ps, the bands are inherently broad, making it difficult to observe the subtle shifts in band frequencies observed previously for the spectra recorded with pulses of nanosecond duration.

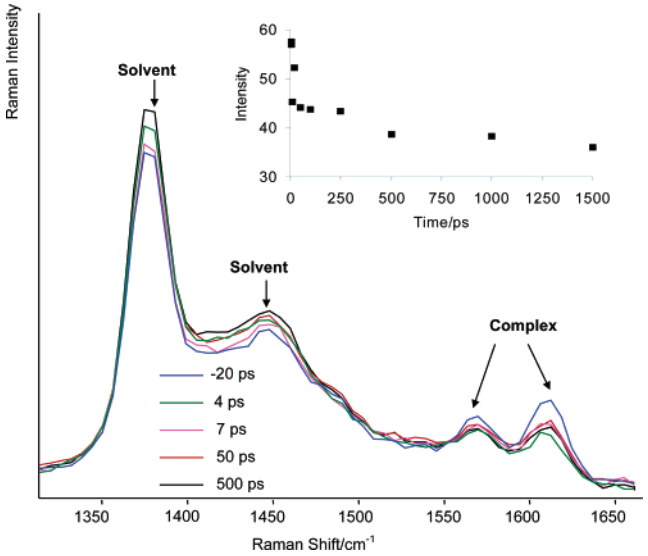

Figure 8. Picosecond-TR^3 study of [Fe(btpa)](PF$_6$)$_2$ in acetonitrile (pump = 390 nm, 10 μJ; probe = 390 nm, 10 μJ). The inset shows the kinetics trace obtained from the scaled subtractions of the data.

Nevertheless, some dynamic effects are evident on the picosecond time scale. Figure 8 shows the spectra recorded for the [Fe(btpa)](PF$_6$)$_2$ complex in acetonitrile. There is a significant depletion in intensity of the complex bands near 1600 cm^{-1} while the solvent bands display a concomitant increase in intensity. The fact that the complex and the solvent features show opposite directions of change confirms that the effects can be associated with actual structural (vibrational) change, as opposed to effects resulting from transient absorption (inner filter) effects. Although there are far too few data points to permit a proper kinetic analysis, the decay is clearly nonexponential (Figure 8, inset), with at least two steps involved, the faster process being complete in less than 20 ps. Similar series of ps-TR^3 experiments on the benzyl complex [Fe(b(bdpa))](PF$_6$)$_2$, also in acetonitrile solvent, exhibited analogous behavior, with the derived kinetic trace also displaying nonexponential behavior. The latter point contrasts with the observation of a single-exponential decay for this complex in the ns-TR^3 experiments (vide supra).

Picosecond transient absorption measurements were also carried out[28] for both complexes; in each case a bleach of the ground state (^{1}MLCT) absorption band was observed across the (460−660) nm wavelength range investigated, similar to what has been reported for several other SCO systems.[29,30]

Variable-Temperature Resonance Raman Spectroscopy. Variable-temperature resonance Raman spectroscopy was used to compare the changes produced in the vibrational spectra following thermal displacement of the spin equilibrium with those generated by pulsed irradiation and consequent photoperturbation of the equilibrium. The spectra were recorded in deuterated acetonitrile so the upper temperature limit was determined by the boiling point of the solvent. Nevertheless, 345 K was found to be sufficiently high to produce readily detectable changes in the resonance Raman spectra.

However, solutions of the complexes exhibited significant luminescence under the CW excitation conditions used to acquire the resonance Raman spectra, making normal spectral acquisition difficult. To overcome this, a technique[31] for fluorescence background correction in Raman spectra was used.

Although the resulting spectra are considerably more noisy than those obtained by the ns TR^3 method, the main features can be observed and there are significant changes with temperature. The spectrum at room temperature (Figure S4, Supporting Information) matches the probe-only spectrum recorded with pulsed laser excitation (Figure 5, trace g), while the spectrum at higher temperature resembles the spectrum at short time delays in the TR^3 studies, displaying mainly HS features. The scaled subtractions highlight the shifts in the bands during the thermally induced spin crossover. The 1610 cm^{-1} band shifts to 1602 cm^{-1} on going from LS to HS, and there is a corresponding decrease in intensity. In addition, there are small changes in the bands at 1485 and 1331 cm^{-1} which again parallel the shifts evident in the subtracted spectra in the TR^3 study. Spectra for the [Fe(b(bdpa))](PF$_6$)$_2$ (not shown) also reveal that heating induces an increased population of the HS state, analogous to changes seen in the corresponding TR^3 spectra.

Variable-Temperature Surface-Enhanced Resonance Raman Spectroscopy. Spectra were also recorded for the various complexes in colloidal silver solutions, with the aim of exploiting surface-enhanced Raman scattering to improve the signal:noise quality of the spectra.

There are, to our knowledge, no reports in the literature of the application of SERRS to the spin-crossover area. However, there are reports of SERRS studies on other Fe(II) complexes such as [Fe(bpy)$_3$]$^{2+}$ [32a] and [Fe(phen)$_2$(CN)$_2$].[32b,c] The luminescence from [Fe(btpa)](PF$_6$)$_2$ which accompanied acquisition of resonance Raman spectra was significantly reduced, following addition of a small amount (<1 mg) of the solid complex to silver colloid at room temperature (with presumably some fraction of the solid complex going into solution in the colloid). Importantly, comparison of the SERRS spectrum for this sample (Figure 9) with the corresponding RT spectrum of the complex in

(28) The picosecond transient absorption (ps-TA) studies were also performed at the RAL facility. The measurements were carried out using two independently tunable and synchronized 200−300 fs pulses generated by a regenerative amplifier system operated at 800 Hz. The pump pulse was obtained at 400 nm, and a white light continuum was used as a probe. This white light was separated into two beams, one passing through the sample and the other used as a reference; both beams were dispersed onto two identical photodiode arrays. The probe beam was delayed with respect to the pump beam by means of an optical delay line.

(29) Monat, J. E.; McCusker, J. K. *J. Am. Chem. Soc.* **2000**, *122*, 4092.
(30) McCusker, J. K.; Walda, K. N.; Dunn, R. C.; Simon, J. D.; Magde, D.; Hendrickson, D. N. *J. Am. Chem. Soc.* **1993**, *115*, 298.
(31) (a) Bell, S. E. J.; Bourguignon, E. S. O.; Dennis, A. C. *Analyst* **1998**, *123*, 1729. (b) Bell, S. E. J.; Bourguignon, E. S. O.; Dennis, A. C.; Fields, J. A.; McGarvey J. J.; Seddon, K. R. *Anal. Chem.* **2000**, *72*, 234. (c) O'Grady, A.; Dennis, A. C.; Denvir, D.; McGarvey, J. J.; Bell, S. E. J. *Anal. Chem.* **2001**, *73*, 2058.
(32) (a) Dines, T. J.; Peacock, R. D. *J. Chem. Soc., Faraday Trans.* **1988**, *84*, 3445. (b) Janik-Czachor, M.; Jasny, J. *J. Electrochim. Acta* **1992**, *37*, 2347. (c) Corio, P.; Temperini, M. L. A.; Rubim, J. C.; Santos, P. S. *Spectrochim. Acta* **1999**, *55*, 2411.

Table 2. Comparison of Peak Positions for $[Fe(btpa)](PF_6)_2$ Obtained from TR^3, Resonance Raman, and SERRS Spectra

TR^3		resonance Raman		SERRS	
low spin/cm^{-1}	high spin/cm^{-1}	low spin/cm^{-1}	high spin/cm^{-1}	low spin/cm^{-1}	high spin/cm^{-1}
1609	1597	1610	1602	1612	1599
1572	1572	1569	1569	1570	1570
1492	1484	1492	1485	1490	1486
1333	1327	1337	1331	1333	1325
1036	1021			1040	1017

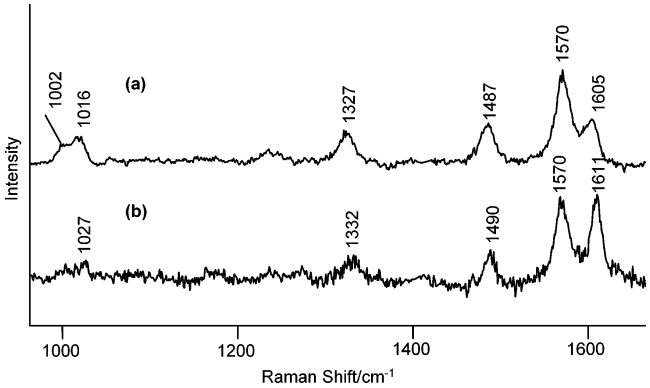

Figure 9. Variable-temperature SERRS of $[Fe(btpa)](PF_6)_2$ + aqueous silver colloid recorded at 514.5 nm: (a) 295 K; (b) 235 K.

homogeneous solution (Figure S4, Supporting Information) shows that a spin-state equilibrium is present in the colloidal environment.[33] In further confirmation of this, cooling of the sample to 235 K (Figure 9b) resulted in a grow-in of the spectral features characteristic of the LS species and the effect was reversible. As a check that a genuine spin-equilibrium was being observed in the colloidal medium, the Raman spectrum of the solid complex alone, in absence of colloid, showed no change upon cooling over the range 298−233 K.

Table 2 compares the peak positions of the LS and HS species obtained from the scaled subtraction spectra recorded under the three types of experimental conditions employed in the present investigation, photoperturbation, variable temperature in homogeneous solution, and variable temperature in colloid. Within experimental error the internal consistency among the spectra is very satisfactory.

Discussion

The Mössbauer data point to the coexistence of approximately equal, *T*-independent fractions of high-spin and low-spin Fe(II) in solid $[Fe(btpa)](PF_6)_2$ recrystallized from dichloromethane/light petroleum[34] (relevant Mössbauer spectra of $[Fe(btpa)](PF_6)_2$ shown in Figure S5, Supporting Information) while the NMR data suggest a dynamic HS−LS interconversion.[24] The six-coordinate isomer is assigned as the low-spin form, while the distorted isomer is assigned as the high-spin species. This is in line with observed differences in bond lengths: all bonds for the distorted isomer are longer than those for the C_2 isomer, the difference being as large as 0.3 Å or greater for the $Fe-N_{bipy}$ bonds. Although the system demonstrates spin equilibrium in solution, there is no indication of spin-crossover behavior in the solid. Seemingly, both spin isomers are trapped in the crystal lattice and interchange is hindered.

The X-ray, Mössbauer, and susceptibility data for solid $[Fe(b(bdpa))](PF_6)_2$ point to a molar fraction of about 0.25 of the high-spin isomer over the whole temperature range and a dynamic interconversion between spin isomers. The latter is evident from the broad lines and the asymmetry of the relatively narrow doublet in the RT Mössbauer spectrum. The apparent discrepancy between the magnetic data and the relative peak area of the HS species may be accounted for by the lower Debye temperature of the latter. Taking into account the fact that the molar fraction of the HS species is about 0.25, as deduced from susceptibility data, our interpretation is that one of the symmetry-independent molecules in the unit cell is low-spin, while another reveals a dynamic disorder between low-spin and high-spin isomers of comparable fractions. Similar dynamic processes have been previously reported.[35]

If we turn to the photoinduced SCO, although the finer details of the early-stage photophysics involved in photoinduced SCO are still not completely established,[6] it is clear that rapid conversion must occur from the initially populated (Franck−Condon) charge-transfer ^{1}MLCT state to the ligand field $^5T_2$ state and ultrafast transient absorption studies by McCusker and co-workers[29,30] on related Fe(II) complexes suggest that this step takes place in <1 ps. The fast bleach observed in the present picosecond TA measurements for both $[Fe(btpa)](PF_6)_2$ and $[Fe(b(bdpa))](PF_6)_2$ is consistent with this conclusion, although the available time resolution precludes any finer investigation of this point at present.

On the time scale of the ns-TR^3 experiments under consideration in this work, it is only the $^5T_2 \rightarrow {}^1A_1$ relaxation which is being probed and the results of the TR^3 studies support this conclusion in that all of the Raman spectral bands assigned to the LS and/or HS isomers are attributable to modes[26] of the neutral bipyridyl ligand which forms the backbone of the btpa ligand. The very good agreement shown in Table 2 in the band positions of the TR^3 spectra with those

(33) Although there is clear spectral evidence for the spin equilibrium in the colloid, it is not possible to state whether the *position* of equilibrium remains the same as in homogeneous solution.

(34) Two doublets of approximately equal integral intensity are observed between 77 and 290 K with typical high-spin (IS 0.88, QS 2.32 mm/s) and low-spin (IS 0.29, EQ 0.42 mm/s, vs Fe) values at RT for a recrystallized sample. The Mössbauer spectrum of the sample obtained directly from synthesis reveals the presence of both the above species as well a second high-spin isomer with IS = 1.25 and QS = 2.80 mm/s at RT. Its magnetic moment is nearly independent of temperature, being 4.24 and 4.57 μ_B at 77 K and RT, respectively. The origin of the second high-spin isomer is unclear at present.

(35) (a) Winkler, H.; Trautwein, A. X.; Toftlund, H. *Hyperfine Interact.* **1992**, *70*, 1083. (b) Adler, P.; Spiering, H.; Gütlich, P. *Hyperfine Interact.* **1988**, *42*, 1035. (c) Adler, P.; Spiering, H.; Gütlich, P. *Inorg. Chem.* **1987**, *26*, 3840. (d) Wolny, J. A.; Toftlund, H. *J. Chem. Soc., Dalton Trans.* Submitted for publication.

recorded in the thermally induced SCO in either homogeneous solution or in the colloidal environment provides further confirmation that the same SCO relaxation is being studied following photoperturbation, as would be the case for the relaxation after thermally induced displacement of the spin equilibrium.

There is no indication in the TR^3 spectra of the presence of any radical anion (bipyridyl$^{\bullet-}$) features which would characterize a charge-transfer MLCT state, nor would such be expected on a nanosecond time scale[36] on the basis of the ultrafast transient absorption studies already referred to.[29,30] The bands which appear at the shortest pump−probe delay times in the ps-TR^3 spectra are also due to neutral ligand modes, so that even on this time scale there is no spectral evidence to suggest that any state other than $^5T_2$ participates in the relaxation step back to $^1A_1$. On the question of the more intimate details of the reaction coordinate for the spin-state relaxation, the band near 1330 cm^{-1} is noteworthy. The mode associated with this feature involves[26] a significant contribution from the stretching coordinate of the central C−C bond of the bipyridyl segment of btpa. The frequency of this band might therefore be taken as a pointer to any structural changes accompanying the spin conversion (e.g. dihedral angle changes involving the bipyridyl moiety) that could be linked to changes in the C−C bond order.[37] In fact, the ns-TR^3 results show that the frequency change in the 1330 cm^{-1} band is small between the LS and HS isomers (<5 cm^{-1}), suggesting that a twisting coordinate involving dihedral angle changes does not contribute to the spin-crossover coordinate to any significant degree. This conclusion is in accord with the findings from the X-ray structural analysis. Moreover, the fact that virtually identical Raman spectral changes accompany the nanosecond-TR^3 dynamics in both $[Fe(btpa)](PF_6)_2$ and the benzyl analogue, $[Fe(b(bdpa))](PF_6)_2$, tends to eliminate any intimate involvement of the pyridyl arms in the relaxation mechanism.

For the band near 1040 cm^{-1} in the spectrum of the LS isomer, the substantial downshift to 1023 cm^{-1} observed in the spectrum of the HS species might suggest a significant contribution to the mode responsible from a coordinate such as a C−N stretching coordinate which couples to the Fe−N bond length changes accompanying spin crossover. However, if such a mode were involved, it would be necessary then to conclude that σ-back-bonding effects are more important than π-back-bonding to account for the decreased frequency in the HS isomer. DFT computational studies are currently in progress to investigate the nature of the vibrational modes.

As previously discussed, McCusker et al. have found that the $^5T_2$ state forms in <1 ps following $^1A_1 \rightarrow {}^1$MLCT excitation in SCO systems.[29,30] In the case of an Fe^{II} polypyridyl complex close to the SCO point, for which the initial ^{1}MLCT−$^5T_2$ ISC is complete in <1 ps, they observed a subsequent slower step with a time constant of 8 ± 3 ps, which was assigned to vibrational cooling in the $^5T_2$ state.[29] While the time scale (<20 ps) of the faster process contributing to the biphasic decay observed in the picosecond-TR^3 experiments described in the present investigation is comparable with the 8 ± 3 ps figure suggested for vibrational cooling, the TR^3 data to hand at present are insufficient to discern the band narrowing or frequency shifting that would be expected to accompany vibrational cooling.

In a previous paper,[1] evidence was presented for the involvement of two distinct HS states in the spin-crossover kinetics of $[Fe(btpa)](PF_6)_2$, one of which differs from the LS form only in the Fe−L bond length, while the other involves an additional rearrangement of the pendant pyridyl arms. Two possible mechanisms were proposed for generation of the transient populations of these two states following initial Franck−Condon excitation into the ^{1}MLCT state. Mechanism 1 envisaged fast ISC to a state HS_A, followed by both direct relaxation to the LS state and relaxation to a second state, HS_B, i.e., a consecutive decay mechanism. A second possibility envisaged fast ISC into both HS_A and HS_B, followed by decay of each to the LS state. Mechanism 1 was favored in being more in accord with the established[29] ultrafast photophysical formation of HS states. The biphasic relaxation which is seen in the picosecond TR^3 experiments might at first sight be taken as also favoring mechanism 1. However, the fact that we also see a biphasic decay in the benzyl complex, where only one type of HS state is involved (cf. the monophasic decay seen in the ns-TR^3 studies), would seem to rule against this conclusion. Further assessment of the possibility of vibrational cooling in these and other SCO systems will require more extensive TR^3 investigations, perhaps complemented by ultrafast time-resolved infrared studies.

Conclusions

The $[Fe(btpa)](PF_6)_2$ complex contains one high-spin and one low-spin molecule in the unit cell, these entities differing significantly in their molecular geometries. In particular, one of the two pyridines which are uncoordinated in the low-spin isomer undergoes a dramatic reorientation on going to the high-spin form. Analysis of the $[Fe(b(bdpa))](PF_6)_2$ complex also reveals the coexistence of both spin isomers in the unit cell, the geometry of the high-spin species apparently corresponding to that observed in the $[Zn(btpa)](PF_6)_2$ complex.

This study reports the first case where it has been possible to follow biphasic kinetics of an iron(II) spin-crossover complex by means of subtle changes in the vibrational degrees of freedom. Surface enhanced resonance Raman spectra have also been used to complement the kinetic picture and assist with the band assignments. Comparison of variable-temperature resonance Raman spectra with the ns-TR^3 data confirm that the dynamic changes observed in the latter experiments do correspond to relaxation of the spin equilibrium. The picosecond-TR^3 data point toward early

(36) The probe wavelength, 321 nm, used in the present experiments would not be in strong resonance with the radical anion, [bipyridyl]$^{\bullet-}$, centered transitions, but if a substantial amount of this species were present, a marked reduction in the intensities of the neutral ligand bands would be expected.

(37) McNicholl, R. A.; McGarvey, J. J.; Al-Obaidi, A. H. R.; Bell, S. E. J.; Jayaweera, P. M.; Coates, C. G. *J. Phys. Chem.* **1995**, *99*, 12268.
(38) Hazell, A.; Simonsen, O.; Werneberg, O. *Acta Crystallogr.* **1986**, *C42*, 1707.

relaxation steps preceding the spin-crossover relaxation but require more extensive study.

Acknowledgment. This work was financially supported by the European Union within the TMR network (Grant ERB-FMRX-CT98-0199). We also acknowledge financial support from Invest Northern Ireland, Grant No. RTD COE 40. The authors thank Dr. P. Matousek and Dr. M. Towrie for their assistance with the picosecond studies at the Central Laser Facility, Rutherford Appleton Laboratory, Chilton, U.K., and the EPSRC for access to the Facility (Grant GR/M45696). C.B. thanks the Department for Employment and Learning (Northern Ireland) for a postgraduate studentship. Financial support from the Carlsberg Foundation and Deutsche Forschungsgemeinschaft (Grant Tr 97/32) is gratefully acknowledged. We thank Dr. J. Rene Beattie for advice concerning multivariate analysis techniques.

Supporting Information Available: Table S1, a summary of crystal data for [Ru(btpa)]$(PF_6)_2$ (**1**), [Fe(btpa)]$(PF_6)_2$ (**2a**−**c**), [Zn(btpa)]$(PF_6)_2$ (**3**), and [Fe(b(bdpa))]$(PF_6)_2$ (**4**), Table S2, magnetic susceptibility data for [Fe(btpa)]$(PF_6)_2$ and [Fe(b(bdpa))]$(PF_6)_2$ complexes, Figure S3, nanosecond-TR^3 spectra of [Fe(btpa)]$(PF_6)_2$ in acetonitrile (concentration ca. 5×10^{-4} mol dm^3; pump = 355 nm, probe = 321 nm; pump−probe time delays over the range −50 to 5000 ns), Figure S4, fluorescence-corrected variable-temperature resonance Raman spectra of [Fe(btpa)]$(PF_6)_2$ in deuterated acetonitrile recorded at 514.5 nm and (a) 298 K and (b) 345 K (inset showing the uncorrected spectrum at 298 K), and Figure S5, Mössbauer spectra of [Fe(btpa)]$(PF_6)_2$, where the sample obtained directly from synthesis is measured at different temperatures and the room-temperature spectrum of the sample is recrystallized from dichloromethane/hexane and the low-intensity doublet observed for the latter is due to an oxidation product arising during crystallization. This material is available free of charge via the Internet at http://pubs.acs.org.

IC049809T